Sound channel in an exponentially stratified ocean, with application to SOFAR

Walter H. Munk

Institute of Geophysics and Planetary Physics, Scripps Institution of Oceanography, La Jolla, California 92037
(Received 12 June 1973)

For much of the World's oceans, the stability of the water column beneath the thermocline is quite well represented by $N^2(z)=g\rho^{-1}\,\partial_z\rho'=N_0^2e^{-2z/B}$, where $\partial_z\rho'$ is the vertical gradient in potential density, $N_0\approx 3$ cycles/h is the surface-extrapolated "Brunt–Väisälä" frequency, and $B\approx 1.3$ km is the stratification scale. This leads to an idealized sound channel

$$C(z)=C_1[1+\epsilon(\eta+e^{-\eta}-1)]=C[1+\epsilon(1/2)\eta^2-(1/6)\eta^3+\ldots]$$

with a minimum velocity at the axis $z=z_1$, $\eta=(z-z_1)/\frac{1}{2}B$ being dimensionless depth relative to z_1. The parameters ϵ, z_1 are explicitly expressed in terms of the five coefficients $\alpha, \beta, \gamma; a, b$ (temperature, salinity, pressure coefficients of C; temperature and salinity coefficients of ρ'), given only the form of $N(z)$ and a representative T, S relation. The up–down asymmetry of the channel, a consequence of the fundamental structure of the oceans, plays a first-order role in the propagation characteristics. As an application, the ray arrivals for an axial source and receiver are computed.

Subject Classification: 30.20.

LIST OF SYMBOLS

$C(z)$, C_1, $\hat{C}$	Sound velocity as function of depth, at channel axis z_1, at ray apex
$\theta(z), \theta_1, 0$	Corresponding ray inclination
$\phi(\theta)$, $\hat{\phi}=\phi(0)$	Function defined by Eq. 16
$\eta=(z-z_1)/\frac{1}{2}B$	Dimensionless distance beneath axis; B is scale depth (1.3 km)
$\epsilon=7.4\times10^{-3}$	Perturbation coefficient (Eq. 14)
$\partial_z(\rho', T', S)$	Gradients in potential density, potential temperature, salinity
a, b	Temperature and salinity coefficients of ρ' (Eq. 3)
α, β, γ	Temperature, salinity, and pressure coefficients of C (Eq. 2)
$\gamma_A=0.0114$ km^{-1}	Adiabatic velocity gradient (Eq. 7)
Tu	T, S relation (Eq. 8)
$N(z)$	Väisälä frequency (Eq. 9)
$R^{\mp}, T^{\mp}, \tau^{\mp}$	Range, travel times, and time delays of upper/lower loops (Eqs. 21, 27)
$R_0=23.7$ km	Range of axial loop (Eq. 22)
$\tau_0=1.41$ sec	Scale of time delay (Eq. 30)
m, n	Number of loops and double loops (Eq. 28)
$L, D, \tilde{L}=L/2R_0$, $\tilde{D}=D/\tau_0$	Total travel distance and time delay (Eqs. 29, 30)

INTRODUCTION

Since the discovery of the oceanic sound channel by Ewing and Worzel[1] it has at times been found useful to idealize $C(z)$ near the velocity minimum. The simplest presentation is by (unequal) linear gradiants of opposite sign above and below the minimum; rays are then arcs of circles. But this has an undesirable kink at the minimum. A parabolic fit avoids the discontinity in $\partial_z C$; for the special case $C=C_1(1-\epsilon\eta^2)^{-1/2}$, with η a dimensionless depth relative to the minimum, the rays are exact sinusoids.[2]

Here the procedure is to *derive* $C(z)$ given an exponential decrease of stratification with depth; the exponential-like decrease (Fig. 1) is perhaps the most intrinsic dynamic property of the abyssal oceans,[3] though an interpretation in terms of fundamental principles has yet to be made.[4] The exponential stratification model leads to

$$C(z)=C_1[1+\epsilon(\eta+e^{-\eta}-1)], \tag{1}$$

with the exponential increase dominating in the upper waters (negative η) and the linear term dominating in deep waters. Pedersen[5] has demonstrated the sensitive dependence of crucial propagation parameters on the profile near the axis. For instance, the distance $R(\theta)$ between axial crossings for a ray loop with axial inclination θ has a *minimum* for $\theta=0$ in the case of the linear profile, a *maximum* for the Eckart profile,[2] and increases monotonically with increasing θ (going from upper to lower loops) for Eq. 1. The up-down asymmetry of Eq. 1 is therefore an essential ingredient to the acoustic properties of the channel; it derives here not from curve fitting, but from the intrinsic difference between deep and shallow ocean processes.

Profile 1 completely ignores the surface mixed layer (deep in winter at high latitude) and irregularities at all depths associated with spreading water masses, down to the scale of microstructure. For an actual case it will always be better to rely on numerical calculation based on the measured profiles. Still the proposed profile may be useful as a canonical description of the gross features at temperate latitudes.

I. SOUND VELOCITY PROFILE

The (fractional) velocity gradient can be written

$$C^{-1}\partial_z C = \alpha\cdot\partial_z T + \beta\cdot\partial_z S + \gamma\cdot\partial_z P, \tag{2}$$

with

$$(\alpha, \beta, \gamma) = C^{-1}\cdot(\partial_T, \partial_S, \partial_P)C\ .$$

Similarly, the fractional density gradient is

$$(\rho')^{-1}\partial_z\rho' = -a\partial_z T' + b\partial_z S\ , \tag{3}$$

with the primes designating potential (observed minus adiabatic) gradients. Second-order terms are neglected in Eqs. 2 and 3. The procedure now is to eliminate temperature and salinity gradients between Eqs. 2 and 3, using Eq. 8 for a T, S relation, leading to the basic equation, Eq. 10.

All coefficients are positive[6]:

$$\begin{aligned} &\alpha = 3.16\times10^{-3}\ (°C)^{-1}, \quad a \approx 0.13\times10^{-3}\ (°C)^{-1},\\ &b = 0.80\times10^{-3}\ (‰)^{-1}, \quad \beta = 0.96\times10^{-3}\ (‰)^{-1},\\ &\gamma = 1.11\times10^{-2}\ \text{km}^{-1}. \end{aligned} \tag{4}$$

The a value is typical of conditions in the sound channel, but may vary by as much as 50% between top and bottom. The γ value is strictly in dimensions of reciprocal pressure (1 km of seawater exerts a pressure of 99 bars).

At great depth the temperature approaches the adiabatic gradient[7]

$$\partial_z T_A = g(\tilde{\gamma}-1)/aC^2 \approx 0.10\ °\text{C/km} \tag{5}$$

($\tilde{\gamma} = 1 + 0.0035$ is the ratio of specific heats), and it is convenient to rewrite Eq. 2 in the form

$$C^{-1}\partial_z C = \alpha\partial_z T' + \beta\partial_z S + \gamma_A, \tag{6}$$

where

$$\begin{aligned} \gamma_A &= \gamma\partial_z P + \alpha\partial_z T_A\\ &= 1.11\times10^{-2} + 0.03\times10^{-2} = 1.14\times10^{-2}\ \text{km}^{-1} \end{aligned} \tag{7}$$

is the fractional velocity gradient in an adiabatic ocean.

The T, S relation is now introduced in terms of the "Turner number"

$$Tu = b\partial_z S/a\partial_z T'\ . \tag{8}$$

Tu is the ratio of the relative contributions of salt and (potential) temperature to the stability of the water column.[8] Combining Eqs. 3, 6, and 8, and using the "Brunt–Väisälä frequency"[7]

TABLE I. Values of $10^6 a$ in $(°C)^{-1}$, at stated temperatures and depths.

	°C					
M	0	5	10	15	20	25
0	51	107	158	204	245	283
1000	76	127	173	216	254	290
2000	100	146	189	227	263	296
3000	122	164	203	238	271	302
4000	143	181	217	249	279	308
5000	161	197	229	258	286	314

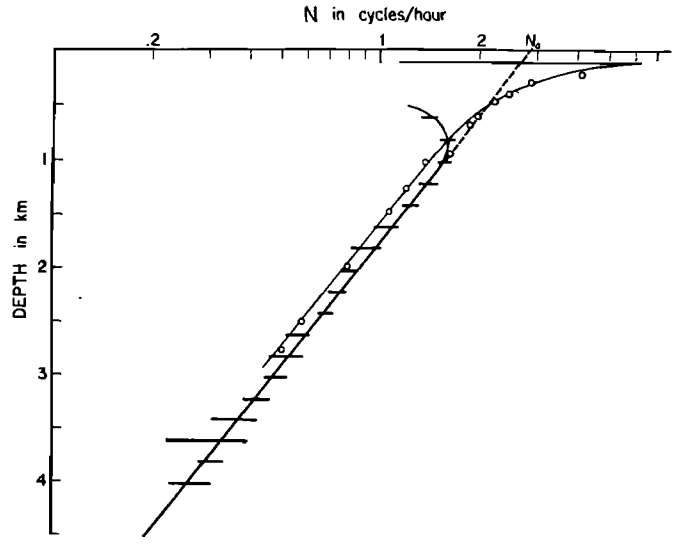

FIG. 1. The Väisälä (or buoyancy) frequency $N(z) = [g\rho^{-1}\partial_z\rho']^{1/2}$. Horizontal bars give range in values measured over the Biscay abyssal plains (46°N 8°W) by Pingree and Morrison.[3] Beneath the thermoclines these have been fitted by $N(z) = N_0 e^{-z/B}$, with $N_0 = 2.8$ cph designating the "surface-extrapolated" value of $N(z)$, and $B = 1.65$ km a "buoyancy scale." In the Pacific ocean (circles) the thermocline is much shallower, typically 100 m, and a "super-exponential" rise takes place between 800 m and the thermoclines.

$$N(z) = [g\rho^{-1}\partial_z\rho']^{1/2} \tag{9}$$

as a measure of the stability of the water column, gives

$$C^{-1}\partial_z C = -(\mu/g)N^2(z) + \gamma_A, \tag{10}$$

with

$$\begin{aligned} &\mu = (\alpha/a)s(Tu), \quad s(Tu) = (1+cTu)/(1-Tu),\\ &\alpha/a = 24.3, \qquad c = a\beta/\alpha b = 0.049\ . \end{aligned} \tag{11}$$

At shallow depth the N^2 term dominates, and the velocity diminishes with depth; at great depth $N^2 \to 0$ and the velocity increases at the rate γ_A. At the axis of the sound channel ($z = z_1$) the condition $\partial_z C = 0$ leads to

$$N(z_1) = N_1 = (\gamma_A g/\mu)^{1/2} = 2.13\times10^{-3}\ \text{s}^{-1/2}\ \text{sec}^{-1} \tag{12}$$

(or $1.22\ \text{s}^{-1/2}$ cycles per hour). For the exponential model $N = N_0 e^{-z/B}$ with $N_0 = 5.24\times10^{-3}\ \text{sec}^{-1}$ (3 cph) and $B = 1.3$ km, the sound axis is at a depth

$$z_1 = B\ln(N_0/N_1) = \tfrac{1}{2}B[\ln(\alpha N_0^2/a\gamma_A g) + \ln s(Tu)]. \tag{13}$$

Using previous numerical values yields

$$z_1 = 1.16\ \text{km} + \tfrac{1}{2}B\ln s$$

compared to typically observed values of 1 to 1.5 km. I shall take $z_1 = 1.3$ km, $B = 1.3$ km.

In terms of a dimensionless depth η reckoned with respect to the sound channel, the solution Eq. 14, using Eq. 12, can be simply written[9]

$$\begin{aligned} &C = C_1[1 + \epsilon(\eta + e^{-\eta} - 1)], \quad \epsilon = \tfrac{1}{2}B\gamma_A = 7.4\times10^{-3},\\ &\eta = (z - z_1)/\tfrac{1}{2}B\ . \end{aligned} \tag{14}$$

This is a reasonable description of an oceanic sound

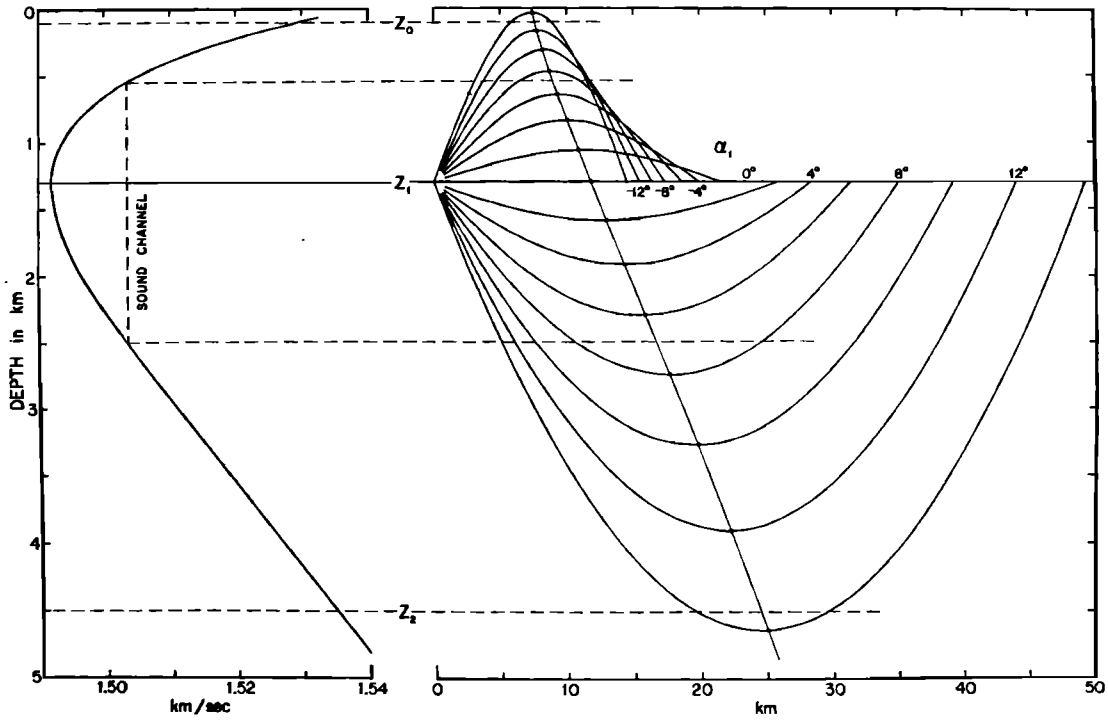

FIG. 2. *Left*: The velocity of sound according to Eq. 1, with $z_1 = B = 1.3$ km, $C_1 = 1.492$ km/sec. *Right*: Numerical ray construction for source on the sound channel axis $z = z_1$. The axial inclinations of the rays (positive downward) are $\theta = -14°$, $-12°$, ..., $12°$, $14°$ ($\hat{\phi} = -2.03$, -1.72, ..., 1.72, 2.03). The surface-limited ray SLR (actually thermocline-limited at $z_0 = 0.1$ km) corresponds to $C_0 = 1.53$ km/sec, $\hat{\phi}_{SL} = -1.855$, $\theta_{SL} = -12.8°$; the bottom-limited ray BLR (for $z_2 = 4.5$ km) to about $\theta_{BL} = +13.6$. The sound-channel, defined by $\hat{\phi}_{SC} = \pm 1$, corresponds to $C_{SC} = 1.503$ km/sec, $\theta_{SC} = \pm 6.9°$, and extends from 0.5 to 2.5 km. The curve $\hat{z}(\hat{x})$ through the ray apexes is nearly linear for this model (Eq. 25).

channel (Fig. 2), given in terms of physical constants of seawater and the stratification parameters N_0, B, Tu. The perturbation coefficient ϵ is readily interpreted as the fractional adiabatic velocity increase over a scale depth.

Geographic variations are associated with the temperature dependence of a (Table I) and the role played by salinity. In freshwater, $Tu = 0$, hence $s(Tu) = 1$, leaving only the first term in Eq. 13. Using $Tu = -0.3$ for North Pacific Intermediate Waters gives $\frac{1}{2} B \ln s = -0.18$ km. Off Bermuda at shallow depth $Tu = 0.8$ and $\frac{1}{2} B \ln s = +1.0$ km. The sound channel is, in fact, shallower in the Pacific than the Atlantic, but the Atlantic s adjustment is too large.

II. RAY ACOUSTICS

Here I follow the formalism developed by Pedersen.[10] From Snell's law

$$C/\cos\theta = C_1/\cos\theta_1 = \hat{C}\,, \tag{15}$$

where $\hat{C}$ is the velocity at the ray apex. Define a dimensionless parameter

$$\phi(\theta) = \mp[(C - C_1)/\epsilon C_1]^{1/2} \tag{16}$$

which varies from $\phi(\theta_1) = 0$ at the axis, to

$$\hat{\phi} = \phi(0) = \mp[(\hat{C} - C_1)/\epsilon C_1]^{1/2} = \sin\tfrac{1}{2}\theta_1/(\tfrac{1}{2}\epsilon\cos\theta_1)^{1/2}$$

at the ray apex ($\theta = \hat{\theta} = 0$). The upper sign refers to a loop *above* the axis (θ, η are positive downward). $\hat{\phi} \ll 1$ for near-axial rays, $\hat{\phi}_{SL} = -1.855$ for the surface-limited ray. But the latter clearly extends beyond the range of the exponential N model (Fig. 1). Somewhat optimistically I will take the model to be applicable within a sound channel "proper," defined by $\hat{\phi} = \mp 1$ (Fig. 2).

Equation 14 can now be written

$$\phi^2(\eta) = \eta + e^{-\eta} - 1 = \sum_{k=2} [(-1)^k/k!]\,\eta^k\,. \tag{17}$$

Equation 17 needs to be "inverted" to express η as function of ϕ. The first term in the expansion, Eq. 17, corresponds to $k = k_0 = 2$. According to the Lagrangian inversion rule η is expanded in powers of $(\phi^2)^{1/k_0}$:

$$\eta = \sqrt{2}\,\phi + \tfrac{1}{3}\phi^2 + (\sqrt{2}/18)\phi^3 + \cdots + b_k\phi^k, \tag{18}$$

with

$$b_k = \frac{1}{k!}\left[\frac{d^{k-1}}{d\eta^{k-1}}\,(\eta^{-2}\phi^2)^{-(1/2)k}\right]_{\eta=0}.$$

Write

$$\frac{dz}{dC} = \frac{\frac{1}{2}B}{\epsilon C_1}\,\frac{d\eta}{d(\phi^2)} = \frac{\frac{1}{2}B}{\epsilon C_1}\,\Phi(\phi), \quad \Phi(\phi) = \sum_{k=1} \tfrac{1}{2} k b_k \phi^{k-2}\,, \tag{19}$$

and define

$$\sin\mu = \phi/\hat{\phi}, \quad 0 \le \mu \le \tfrac{1}{2}\pi\,.$$

The *range* of a ray loop (between axial zero crossings) is given by

$$R = 2\int_0^{\hat{z}} \cot\theta\, dz = 2\int_{C_1}^{\hat{C}} C(\hat{C}^2 - C^2)^{-1/2}(dz/dC)\, dC$$

$$= B\hat{\phi}(2\epsilon)^{-1/2}\int_0^{\pi/2} g(\mu)\Phi(\mu)2\sin\mu\, d\mu\,, \qquad (20)$$

where

$$g(\mu) = [2C^2/C_1(\hat{C}+C_1)]^{1/2} = 1 + \tfrac{1}{4}\epsilon\hat{\phi}^2(3\sin^2\mu - 1) + \cdots$$

varies between $1 - \frac{1}{4}\epsilon\hat{\phi}^2$ and $1 + \frac{1}{2}\epsilon\hat{\phi}^2$ as μ goes from 0 to $\frac{1}{2}\pi$, and can be set $g = 1$ for R of order $\epsilon^{-1/2}$. It follows that

$$R(\hat{\phi}) = B\epsilon^{-1/2}\left[\frac{\pi}{2} + \frac{\sqrt{2}}{3}\hat{\phi} + \frac{\pi}{24}\hat{\phi}^2 + \cdots + \frac{\sqrt{2}}{4}\pi^{1/2}kb_k\frac{\Gamma(\tfrac{1}{2}k)}{\Gamma(\tfrac{1}{2}k+\tfrac{1}{2})}\hat{\phi}^{k-1}\right]\,. \qquad (21)$$

Upward loops ($\hat{\phi}$ negative) have shorter ranges, downward loops have longer ranges, as compared to the range

$$R_0 = R(0) = \tfrac{1}{2}B\pi\epsilon^{-1/2} = 23.7\ \text{km} \qquad (22)$$

of the *axial loop*. The range of a double loop

$$R^- + R^+ = 2R_0(1 + \tfrac{1}{12}\hat{\phi}^2 + \cdots) \qquad (23)$$

always *exceeds* that of the axial ray. The distance $2R_0 = 47.4$ km can be associated with the convergence zone, and the smallness of the $\hat{\phi}^2$ coefficient (e.g., $\frac{1}{12}$) implies that $R^- + R^+$ has a weak dependence on ϕ, and so is a measure of the goodness of convergence. Eliminating $\hat{\phi}$ between Eqs. 21 and 17 yields

$$\hat{\eta} = \frac{\hat{z}-z_1}{\frac{1}{2}B} = \left(\frac{3\pi}{2}\frac{R-R_0}{R_0}\right) - \left(\frac{\pi}{16} - \frac{1}{6}\right)\left(\frac{3\pi}{2}\frac{R-R_0}{R_0}\right)^2 + \cdots\,. \qquad (24)$$

The smallness of the coefficient $\pi/16 - 1/6 = 0.030$ implies a very good fit to the linear relation, as apparent also from Fig. 2:

$$\hat{z} = z_1 + \tfrac{3}{2}\epsilon^{1/2}(R - R_0) = 1.3\ \text{km} + 0.129\ (R - 23.7\ \text{km}). \qquad (25)$$

This linear relation between the height and length of loops, 130 m per km in excess of the range of the axial loop, could be a useful rule of thumb.

The *travel time* along a ray between 0 and R is given by

$$T = 2\int_0^{\hat{z}} C^{-1}\csc\theta\, dz = 2\hat{C}\int_{C_1}^{\hat{C}} C^{-1}(\hat{C}^2 - C^2)^{-1/2}(dz/dC)\, dC$$

$$= \frac{R}{C_1} + 2\int_{C_1}^{\hat{C}}\left(\frac{\hat{C}}{C} - \frac{C}{C_1}\right)(\hat{C}^2 - C^2)^{-1/2}(dz/dC)\, dC\,. \qquad (26)$$

Using $\hat{C}/C - C/C_1 = \epsilon\hat{\phi}^2[C_1/C - \sin^2\mu(C + C_1)C]$ and the expansion $C_1/C = 1 - \epsilon\hat{\phi}^2\sin^2\mu(C_1/C)$ which is derivable from Eq. 16, one obtains

$$\hat{C}/C - C/C_1 = \epsilon\hat{\phi}^2[1 - \sin^2\mu(C + C_1)/C] \approx \epsilon\hat{\phi}^2[1 - 2\sin^2\mu + \cdots]\,.$$

Writing

$$h(\mu) = [2C_1/(\hat{C}+C_1)]^{1/2} = 1 - \tfrac{1}{4}\epsilon\hat{\phi}^2(1 - \sin^2\mu) + \cdots \approx 1,$$

gives

$$\tau = T - \frac{R}{C_1} = \frac{B}{C_1}(\tfrac{1}{2}\epsilon)^{1/2}\hat{\phi}^3\int_0^{\pi/2} h(\mu)\Phi(\mu)(1 - 2\sin^2\mu)2\sin\mu d\,\mu$$

$$= -\frac{B}{C_1}\epsilon^{1/2}\left[\frac{\sqrt{2}}{9}\hat{\phi}^3 + \frac{\pi}{48}\hat{\phi}^4 + \cdots + \frac{\sqrt{2}}{4}\pi^{1/2}\times\frac{k(k-1)}{k+1}b_k\frac{\Gamma(\tfrac{1}{2}k)}{\Gamma(\tfrac{1}{2}k+\tfrac{1}{2})}\hat{\phi}^{k+1}\right]\,, \qquad (27)$$

for the *delay* relative to axial propagation.

Upper loops are delayed, lower loops are advanced relative to the axial arrival. For a double loop, $\tau^- + \tau^+$ is always negative, so the axial ray is the last to arrive. (This is not a universal property of sound channels.[9]) The fact that the expansion for $\tau^- + \tau^+$ starts with a term in $\hat{\phi}^4$ implies that near-axial rays will come in almost on top of one another, as observed in the *finale* of a SOFAR transmission.

III. SOFAR

Collecting formulae,

$$\begin{aligned} R(\hat{\phi}) &= R_0[1 + (2\sqrt{2}/3\pi)\hat{\phi} + \tfrac{1}{12}\hat{\phi}^2]\,, \\ \tau(\hat{\phi}) &= -BC_1^{-1}\epsilon^{1/2}[(\sqrt{2}/9)\hat{\phi}^3 + (\pi/48)\hat{\phi}^4]\,. \end{aligned} \qquad (27)$$

Let there be m^- upper loops and m^+ lower loops, and so $n = \frac{1}{2}(m^- + m^+)$ double loops. There are four cases:

even number of loops
last loop up or down $m^- = m,\ m^+ = m,\ n = m = 1, 2, \ldots,$

odd number of loops
last loop up $m^- = m+1,\ m^+ = m,$
last loop down $m^- = m,\ m^+ = m+1,$ $\quad n = m + \tfrac{1}{2} = \tfrac{1}{2}, \tfrac{3}{2}, \ldots\,.$ (28)

(The two even cases are degenerate if the fluid is horizontally homogeneous.) Thus

$$\begin{aligned} L &= m^-R^- + m^+R^+ = m(R^- + R^+) + \langle R^\mp\rangle \\ D &= T - L/C_1 = m^-\tau^- + m^+\tau^+ = m(\tau^- + \tau^+) + \langle\tau^\mp\rangle \end{aligned} \qquad (29)$$

are total distance and delay, with $\langle\,\rangle$ set to zero for the even number of loops. Using the collected formulas,

$$\begin{aligned} \tilde{L} &= L/2R_0 = (n/12)\hat{\phi}^2 + \langle(\sqrt{2}/3\pi)\hat{\phi}\rangle + n\,, \\ 2R_0 &= \pi B\epsilon^{-1/2} = 47.4\ \text{km} \\ \tilde{D} &= D/\tau_0 = -(1/144)n\hat{\phi}^4 - \langle(\sqrt{2}/54\pi)\hat{\phi}^3\rangle, \\ \tau_0 &= 6\pi\epsilon^{1/2}BC_1^{-1} = 1.41\ \text{sec}. \end{aligned} \qquad (30)$$

These are plotted in Figs. 3 and 4. Elimination of n leads to the linear relation

$$\tilde{D} = -\frac{\hat{\phi}^4}{12(12+\hat{\phi}^2)}\tilde{L} - \left\langle\frac{\sqrt{2}\,\hat{\phi}^3(24-\hat{\phi}^2)}{108\pi(12+\hat{\phi}^2)}\right\rangle\,. \qquad (31)$$

For the sound channel,[11] $\hat{\phi} = \mp 1$, and

$$\tilde{D}^\mp_{SC} = -0.0064\,\tilde{L} \pm \langle 0.0074\rangle\,, \qquad (32)$$

with the upper sign corresponding to the last loop up. Dimensionally, $D^\mp_{SC}\,(\text{msec}) = -0.19L\,(\text{km}) \pm \langle 10.4\rangle$. For the surface-limited ray (beyond the scope of the model) the relation is $D^\mp_{SL}\,(\text{msec}) = -1.90L\,(\text{km}) \pm \langle 50.0\rangle$, thus indicating that the sound-channel arrivals constitute the last 10% of the SOFAR record.

Eliminating $\hat{\phi}$ leads to the arrival delays for specified numbers of loops. For an *even* number of loops,

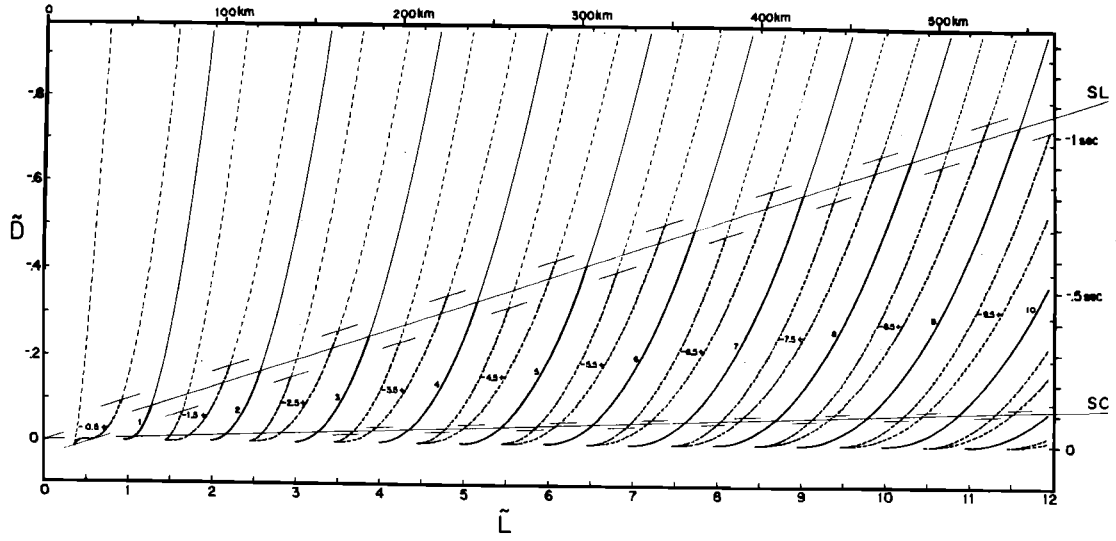

FIG. 3. The arrival delay $\tilde{D}=D/\tau_0$ for various rays as function of the distance $\tilde{L}=L/2R_0$ between a source and receiver on the sound axis. (Dimensional scales correspond to $\tau_0=1.41$ sec and $2R_0=47.4$ km.) Negative values of D indicate arrival prior to the axial arrival. The number of double loops is marked, with solid curves corresponding to an integral number of double loops and dashed curves to an extra upper (minus) or lower (plus) loop. The upper loop is the first to arrive. Sound-channel arrivals are limited to the narrow sector between $\tilde{D}=0$ and the solid-dashed lines labeled SC; similarly SL marks the limit of totally refracted arrivals as determined by the surface-limited ray. Details for the cusps near $\tilde{D}=0$ and $\tilde{L}=0.5$, 1.5 are shown in Fig. 4.

$$\hat{\phi}^2=12(\tilde{L}-n)/n, \quad \tilde{D}=-(\tilde{L}-n)^2/n, \quad n=1,2,\ldots, \quad . \tag{33}$$

Suppose $\tilde{L}$ is an integer, so that

$$n=\tilde{L}, \quad \hat{\phi}=0, \quad \tilde{D}=0$$

corresponds to the final axis arrival. Then for the immediately preceding arrivals,

$$n=\tilde{L}-1, \quad \hat{\phi}^2=12/(\tilde{L}-1), \quad \tilde{D}=-1^2/(\tilde{L}-1),$$
$$n=\tilde{L}-2, \quad \hat{\phi}^2=2\times12/(\tilde{L}-2), \quad \tilde{D}=-2^2/(\tilde{L}-2),$$

etc., so that for distant transmission, $\tilde{D}\approx0$, $-\tilde{L}^{-1}$, $-4\tilde{L}^{-1}$, ..., etc. Should the source and receiver lie some small distance η^* from the axis, then the limiting ray is one that is as nearly as possible horizontal at source and receiver; from (17) $\hat{\phi}^*\approx2^{-1/2}\eta^*$ and $n^*=\tilde{L}/(1+\hat{\phi}^{*2}/12)$. The foregoing sequence starts with the largest integer $n\leq n^*$.

Take $\tilde{L}=100$ ($L=4740$ km) with source and receiver on the axis. For a surface-extrapolated canonical profile, the earliest refracted arrival at

$$\tau=-1.9\times10^{-3}\times4740=-9 \text{ sec}$$

consists of (Eq. 33)

$$n_{SL}=\tilde{L}/(1+\phi_{SL}^2/12)=78$$

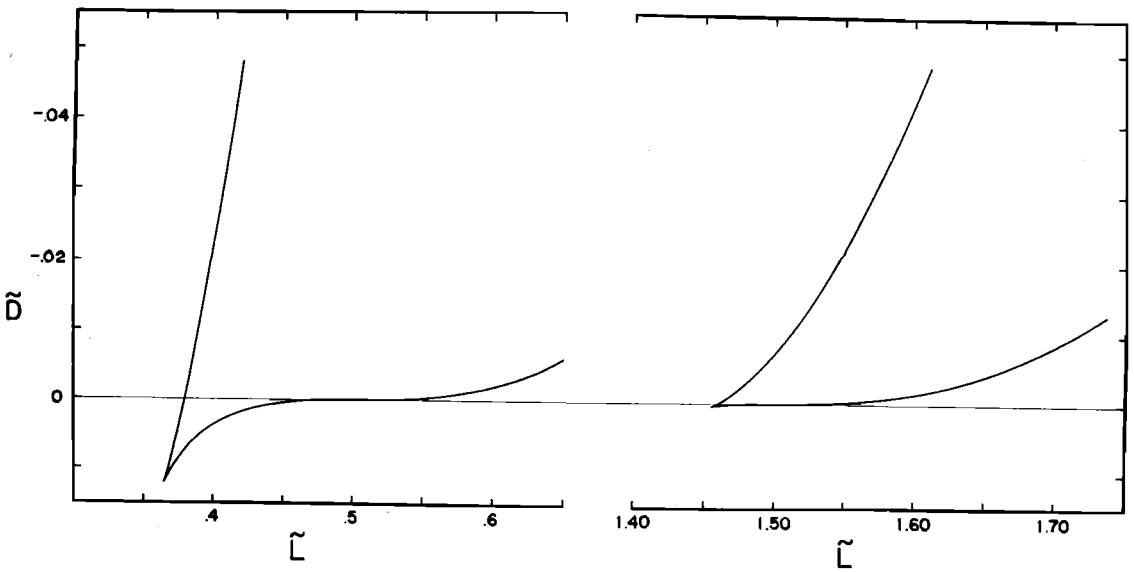

FIG. 4. Details for the arrival of 0.5 double loops (left) and 1.5 double loops (right).

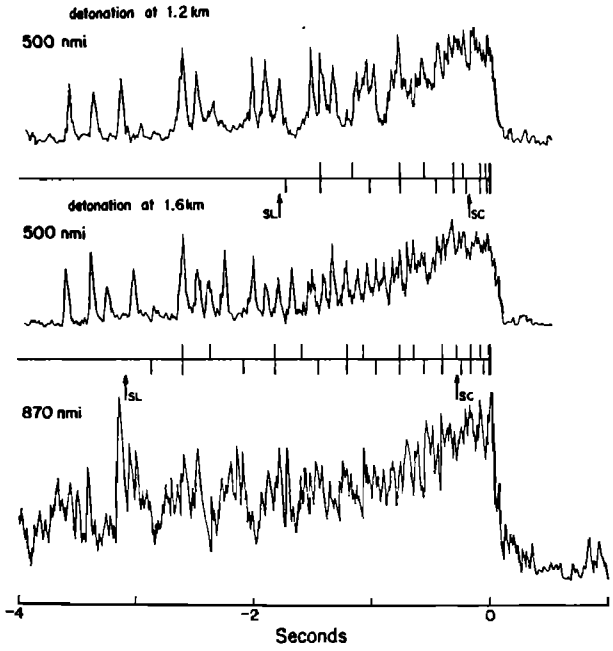

FIG. 5. SOFAR-grams in the Bermuda area for transmission range of 500 naut. miles (TOP and CENTER) and 870 naut. miles (BOTTOM), respectively. Vertical bars give times of computed arrivals (for $B=1.3$ km); upper (lower) bars indicate an odd number of loops, with last loop up (down), double bars indicate an even number of loops. Times of the sound-channel and surface-limited rays are marked. Records by courtesy of Gordon Hamilton and Carl Hartdegen.

double loops. The sound channel (proper) starts with $\tau = -0.19\times10^{-3}\times4740 = -0.9$ sec and 93 double loops, and ends at $\tau = 0$ with $\tilde{L} = 100$ double loops. There is a total of 23 even-loop arrivals, 8 of them in the sound channel proper. The time interval between the last two arrivals is $\tau_0/\tilde{L} = 14$ msec. For source and receiver 500 m off axis, $\eta^* = 0.38$, $n^* = 99.4$, the $n = 100$ arrival is missing, and the last interval is $3\tilde{\tau}_0/\tilde{L} = 52$ msec.

The odd loop arrivals fall between the corresponding even arrivals, with the extra up-loop always preceding the extra down-loop. At the *finale*, the arrivals merge at a cusp (Fig. 4)

$$\hat{\phi} = -2\sqrt{2}/\pi n, \quad \tilde{L} = n - 2/3\pi^2 n, \quad \tilde{D} = 4/27\pi^4 n^3,$$
$$n = \tfrac{1}{2}, \ \tfrac{3}{2}, \ \ldots, \qquad (34)$$

which is (insignificantly) *delayed* relative to the axial arrival. (The interpretation goes beyond ray acoustics.) For large $\tilde{L}$ near the *finale*

$$\tilde{D}^{\mp} = -\frac{(\tilde{L}-n)^2}{n} - \frac{8(\tilde{L}-n)}{3\pi^2 n^2} + \cdots \pm \frac{8\sqrt{6}}{9\pi n^{3/2}}(\tilde{L}-n)^{3/2} + \cdots,$$
$$n = \tfrac{1}{2}, \ \tfrac{3}{2}, \ \ldots, \qquad (35)$$

so that the branches spread at a rate proportional to $(\tilde{L}-n)^{3/2}$. Under ideal conditions these could provide a Vernier scale for variable distance within a convergence zone. At earlier times, odd and even arrivals are evenly spaced, so that a sequence of arrivals n, $(n+\frac{1}{2})^-$, $(n+\frac{1}{2})^+$, $n+1$, ..., can be represented by the formulas 33 with n, $n+\frac{1}{3}$, $n+\frac{2}{3}$, $n+1$, ... The interval between successive arrivals (in τ_0 units) is then

$$\frac{1}{3}\frac{\delta\tilde{D}}{\delta n} = \frac{1}{3}\frac{L^2-n^2}{n^2} = \frac{1}{3}\frac{\phi^2(\phi^2+24)}{144}, \qquad (36)$$

or 0.219 (0.308 sec) for ϕ_{SL}, and 0.058 (0.082 sec) for ϕ_{SC}.

Porter[12] finds $\tilde{D} = -(\pi/6)^2\tilde{L}^3/n^2$ (in my notation) for a bilinear velocity profile, in sharp contrast to the present result $\tilde{D} = -(\tilde{L}-n)^2/n$. Evidently the arrival pattern is critically dependent on the shape of the velocity profile.

IV. OBSERVATIONS

Figures 5 and 6 show some observed and computed arrival sequences. The computed sequences include also arrivals prior to what has been defined as sound-channel proper, and this is particularly questionable for Atlantic transmissions where the thermocline extends all the way to 700 m. Early observed arrivals are clearly associated with this deep and relatively slow mixed layer.

I have used $B = 1.3$ km throughout. For the eastern Atlantic $B = 1.65$ km gives a better fit (Fig. 1); curve fitting in the Bermuda sound channel suggests $B = 0.5$ km. Arrivals near the *finale* have time intervals proportional to

$$\tilde{L}^{-1}\tau_0 = L^{-1}2R_0 \cdot \tau_0 = 6\pi B^2 L^{-1} C_1^{-1} \qquad (37)$$

and are thus subject to considerable geographic variations.

The records reproduced here are the simplest I could find; yet they do not exhibit the clean pattern of arrivals to be expected from an idealized sound channel (and when numerical comparison is attempted, the results are unsatisfactory). I interpret this situation as

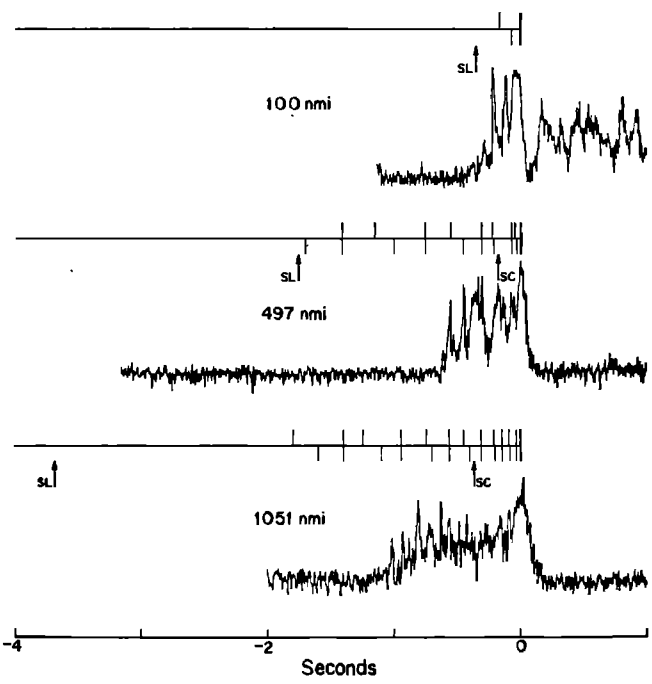

FIG. 6. Pacific SOFAR-grams, by courtesy of W. H. Thorp.

challenging rather than disappointing. While it would have been pretty to find SOFAR-grams in accord with a canonical sound profile, this would have meant that not much more is to be gained from sound propagation studies. The observed discrepancies attest to the power of the acoustical inverse problem: to employ the propagation measurements for observing and describing the real ocean. I suspect the complexity of SOFAR-grams is related to horizontal gradients and to a microstructure in sound velocity that inevitably is superposed on the gross profile, in line with recent findings of a microstructure in temperature and salinity at all depths.[13]

ACKNOWLEDGMENTS

F. Spiess suggested looking for an analytical solution to the sequence of SOFAR arrivals. I am grateful to M. Ewing, F. Fisher, G. Hamilton, C. Hartdegen, J. Northrop, and W. Thorp for information concerning SOFAR-grams. B. Hersey, C. Spofford, and the reviewer have suggested numerious improvements to the manuscript. ONR has supported this work.

[1]M. Ewing and J. L. Worzel, "Long-range Sound Transmission," Geol. Soc. Am. Mem. **27**, Part III (1948).
[2]C. Eckart, "A Simple Sound Channel," MPL Technical Memorandum 211 (Feb. 1970).
[3]C. Garrett and W. Munk, Geophys. Fluid Dynam. **2**, 225 (1972), particularly Fig. 1, based on the work by J. L. Reid and R. J. Lynn, Deep-Sea Res. **18**, 1063 (1971); see also R. D. Pingree and G. K. Morrison, J. Phys. Oceangr. (to be published).
[4]W. H. Munk, Deep-Sea Res. **13**, 707 (1966).
[5]M. A. Pedersen, J. Acoust. Soc. Am. **43**, 619 (1968).
[6]α, β, γ from I. Tolstoy and C. S. Clay, *Ocean Acoustics* (McGraw-Hill, New York, 1966), p. 6, based on W. D. Wilson, J. Acoust. Soc. Am. **23**, 1357 (1960). A more recent evaluation is given by V. A. Del Grosso, J. Acoust. Soc. Am. **53**, 1384 (1973). Table I is adapted from A. Bradshaw and K. E. Schleicher, Deep-Sea Res. **17**, 691 (1970).
[7]C. Eckart, *Hydrodynamics of Oceans and Atmospheres* (Pergamon, Oxford, 1960), p. 6.
[8]The important role played by this ratio is implicit in the work of J. S. Turner, *Buoyancy Effects in Fluids* (Cambridge U. P., 1972), Chap. 8. In North Pacific Intermediate Waters $Tu = -0.3$. The Mediterranean outflow into the North Atlantic gives rise to irregularity in $Tu(z)$ near the sound axis; a typical value of Bermuda is $Tu = +0.8$.
[9]More precisely $C/C_1 = \exp[\epsilon(\eta + e^{-\eta} - 1)]$, which differs from Eq. 14 by terms of order $\epsilon^2\eta^4$.
[10]M. Pedersen, J. Acoust. Soc. Am. **45**, 157 (1969).
[11]But note the relatively slow convergence of the expansions, Eqs. 21 and 27 for $\hat{\phi}$ of order 1. For large k, the coefficients in $\hat{\phi}^k$ diminish as $(k/e)^{-k}$.
[12]R. P. Porter, J. Acoust. Soc. Am. **53**, 181 (1973), Eq. 3. For comparison, I have equated his $q_e = 2.08 \times 10^{-2}$ km^{-1} to $2\gamma_A = 2.28 \times 10^{-2}$ km^{-1}.
[13]M. C. Gregg and C. S. Cox, Deep-Sea Res. **19**, 355 (1972).